TWO-NUCLEON EMISSION WITH POLARISED PHOTONS

I.J.D. MacGregor[1, †]

(For the PiP/TOF group of the Mainz A2 collaboration)

[1] *Department of Physics and Astronomy, University of Glasgow, Glasgow, UK*

The ^{12}C($\vec{\gamma}$,pp) and ^{12}C($\vec{\gamma}$,pn) reactions have recently been measured in the Δ-resonance region using linearly polarised tagged photons. The experiments used the Glasgow tagged-photon spectrometer [1] at the Mainz 855 MeV electron microtron MAMI [2]. Data corresponding to the direct emission of nucleon pairs from $(1p)^2$ and (1p)(1s) orbits were selected using missing energy and angular cuts. The experiments investigated the photon energy, missing energy, recoil momentum and angular dependences of the Photon Asymmetry Σ and the cross sections $\sigma_{\parallel}$ ($\sigma_{\perp}$) for events emitted parallel (or perpendicular) to the plane of polarisation of the incident photons. The data are compared with state-of-the-art calculations of direct two-nucleon emission using the model developed by the Gent theory group [3]. The experimental data reveal important features which were not accessible to previous experiments with unpolarised photons. In particular, the ^{12}C($\vec{\gamma}$,pp) reaction shows a strong (negative) peak in Σ at missing energies just above the reaction threshold, which is interpreted as new evidence of a direct photoproduction process for this reaction channel. The theoretical calculations reproduce some of the general trends of the measured data, but do not agree in detail with the experimental spectra. At high missing energies, for E_γ>250 MeV, where two-step processes dominate, Σ has a substantial negative value for both reaction channels. This is attributed to a strong asymmetry in the initial photon absorption process.

1. INTRODUCTION

Polarised photon experiments provide a unique and relatively new tool to explore the mechanisms contributing to photoinduced two-nucleon knockout reactions [3, 4]. For instance, polarised photon experiments can measure cross sections for reactions in which the polarisation of the incident photon is parallel ($\sigma_{||}$) or perpendicular ($\sigma_{\perp}$) to the reaction plane. The photon asymmetry (Σ), defined by $\Sigma = \frac{\sigma_{\parallel} - \sigma_{\perp}}{\sigma_{\parallel} + \sigma_{\perp}}$, emphasises the differences between $\sigma_{||}$ and $\sigma_{\perp}$ but is insensitive to the similarities.

The photonuclear response is expressed through the transverse structure functions $W_T = W^{xx} + W^{yy}$ and $W_{TT} = W^{xx} - W^{yy}$. The unpolarised cross section is simply proportional to W_T, which gives an average of the parallel and perpendicular nuclear response, whereas the photon asymmetry can access the differences contained in W_{TT} through the relation $\Sigma = -\frac{W_{TT}}{W_T}$.

The mechanisms contributing to (γ,pn) reactions include Meson Exchange Current (MEC) contributions, Δ-currents, central and tensor Short Range Correlations (SRC) and Final State Interactions (FSI) [3, 4]. In the (γ,pp) reaction the main contributions arise from Δ-currents, Central SRC and FSI, since the contributions from charge-exchange MEC and tensor SRC are suppressed. These various mechanisms are sensitive in differing degrees to nuclear density, nucleon angular momentum states and photon polarisation. In particular, W_{TT} is known to be sensitive to angular momentum quantum numbers and to interference between the contributing processes [3, 4].

The present ^{12}C($\vec{\gamma}$,pp) and ^{12}C($\vec{\gamma}$,pn) measurements were carried to study the sensitivity of photonuclear two-nucleon emission reactions to polarisation degrees of freedom. Some selected results from this experiment have already been reported [5–7]. This paper presents additional experimental data and makes comparisons with more detailed theoretical calculations than previously presented.

[†] Electronic address: i.macgregor@physics.gla.ac.uk;
URL: http://www.physics.gla.ac.uk/~ianm/

2. EXPERIMENT

The layout of the experiment is shown in Fig. 1. It was carried out using the Glasgow tagged-photon spectrometer [1] at the Mainz 855 MeV electron accelerator MAMI [2].

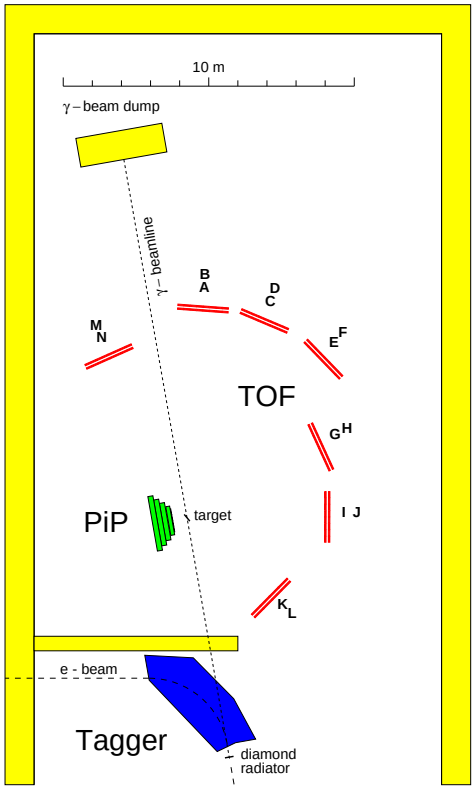

Fig. 1: Experimental layout of the Mainz A2 Hall. Linearly polarized photons, produced by coherent bremsstrahlung in a thin diamond radiator, are tagged in the Glasgow tagged-photon spectrometer [1]. Three different diamond orientations were used to produced polarised photons in the range E_γ=160–350 MeV. Protons from reactions in the ^{12}C target are detected in the scintillation hodoscope PiP [8]. Correlated neutrons and protons are detected in the array of time-of-flight scintillation detectors TOF [9].

A 100 μm thin, low-mosaic diamond radiator was used to produce coherent bremsstrahlung by aligning the crystal to scatter electrons off the $[02\bar{2}]$ reciprocal lattice vector. The photon beam was collimated to a half angle of 0.6 mrad to select the highest polarisation part of the coherent bremsstrahlung angular distribution. The energy width of the coherent bremsstrahlung peak was ~70 MeV FWHM, so three separate measurements with different crystal alignments were used to cover the E_γ range 160–350 MeV. The plane of polarisation was rotated periodically through 90° to minimise systematic errors.

The polarisation P of the photon beam was calculated using a Monte Carlo code [10] incorporating both the coherent and incoherent bremsstrahlung processes. The code takes into account the divergence of the incident electron beam, multiple scattering of the electron beam in the diamond radiator, the temperature dependence of the bremsstrahlung production processes and collimation of the photon beam. It includes contributions from the 20 strongest reciprocal lattice vectors.

In the data analysis E_γ bins with high values of photon polarisation, and tagging efficiency, were selected. The regions chosen were on the low energy side of the polarisation peak where the calculation of P is least sensitive to uncertainties in the parameters describing the electron beam and the diamond radiator. In total six E_γ bins: 160–190, 190–220, 220–250, 250–280, 290–320 and 320–350 MeV were used. These had average P values of 49.0%, 66.7%, 50.0%, 60.5%, 37.1% and 49.5%, respectively.

In the experiment the polarised photons were incident on a 0.5 g/cm^2 graphite target mounted at 30° to the photon beam line. Protons from reactions in the target were detected in PiP [8], a ~1 sr solid angle plastic scintillation hodoscope covering polar angles from 50° to 130° and azimuthal angles of ±22° . The range of PiP proton energies accepted in the analysis was 31–330 MeV.

Correlated protons and neutrons were detected in TOF [9], an array of plastic scintillator detectors used to measure particle energies by the time-of-flight technique. TOF bars (20 cm wide×5 cm

thick×3 m high) were mounted on stands 8 bars wide, 2 layers deep. The TOF stands were placed to cover a wide range of polar angles with flight-paths from ∼4.5 m to ∼7.5 m. Using two layers of TOF stands increased the neutron detection efficiency by a factor of ∼2. For neutrons the TOF pulse height thresholds were set at 17 MeV (9 MeV_{ee}), which gave a neutron detection efficiency of ∼9% for the double layers. For protons the pulse height threshold used corresponded to ∼40 MeV at the target, after the effects of energy losses in the target and the air were taken into account.

Further details of the experiment and data analysis are given in [5, 7].

3. THEORETICAL CALCULATIONS

The experimental data are compared with predictions of a theoretical model of direct two-nucleon knockout developed by the Gent group [3]. The model calculates parallel and perpendicular cross sections in an unfactorised distorted wave treatment of the interaction. It includes pion exchange and Δ-isobar currents and incorporates short-range interactions using a central correlation obtained from a G-matrix calculation by Gearhart and Dickhoff [11]. The effects of tensor correlations have also been included.

The calculations used a Monte Carlo technique developed by Ireland *et al.* [12] to average over the acceptance of the experimental detectors. Ireland *et al.* have shown that significant variations in cross section can occur within relatively small angular bins and that cross sections evaluated for "central" kinematic conditions for a particular bin can be significantly different from the average over that bin. Effects are also seen in the calculation of Σ for both reaction channels, but in this case the differences between the average values and the "central point" values are generally small.

Separate calculations were made for two-nucleon emission from each possible combination of the contributing neutron and proton $1p_{3/2}$, $1p_{1/2}$ and $1s_{1/2}$ nucleon subshells. The data were initially compared with calculations of the dominant $(1p_{3/2})^2$ and $(1p_{3/2})(1s_{1/2})$ contributions to the $(1p)^2$ and (1p)(1s) missing energy regions. However to provide more detailed insight into the effects of shell structure, comparisons were also made with predictions obtained by combining all of the possible subshell contributions to each of the $(1p)^2$ and (1p)(1s) E_m regions using spectroscopic factors derived from ^{12}C(e,e'p) reactions [13].

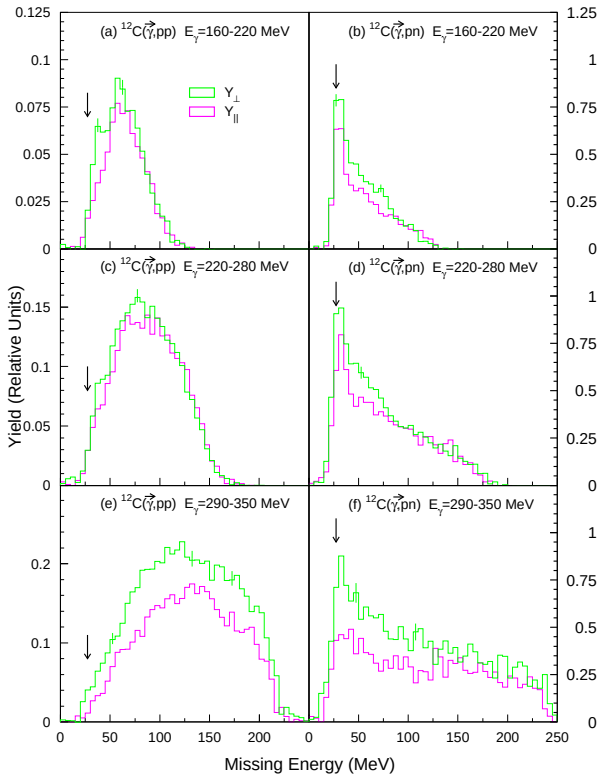

Fig. 2: ^{12}C(γ,pp) and ^{12}C(γ,pn) Missing Energy spectra for photons polarised perpendicular (green) or parallel (purple) to the detector plane, for three photon energy ranges. The arrows indicate the reaction thresholds.

4. RESULTS

A Missing Energy Dependence

Fig. 2 shows E_m spectra for the $^{12}C(\vec{\gamma},pp)$ and $^{12}C(\vec{\gamma},pn)$ reactions for events detected in all of PiP and TOF, for three E_γ ranges. Separate spectra are shown for data in which the photon polarisation is parallel or perpendicular to the plane of the detectors.

In the (γ,pn) channel the strong peak previously observed in unpolarised experiments, just above the reaction threshold [14, 15, 17], is evident in both the parallel and perpendicular data sets. This peak has been attributed to direct two nucleon knockout processes which leave the residual nucleus in relatively low lying excited states. The strength of the peak is stronger in the perpendicular data at all photon energies.

In contrast the (γ,pp) channel shows relatively little strength at low E_m, but a distinct shoulder at E_m ~40 MeV is evident in the perpendicular yield in the lowest two E_γ ranges. An indication of some structure at these missing energies was first noticed by Harty *et al.* in previous work with unpolarised photons [17]. However, this feature is much more distinct in the present work and is now clearly seen to be associated with the perpendicular nuclear response.

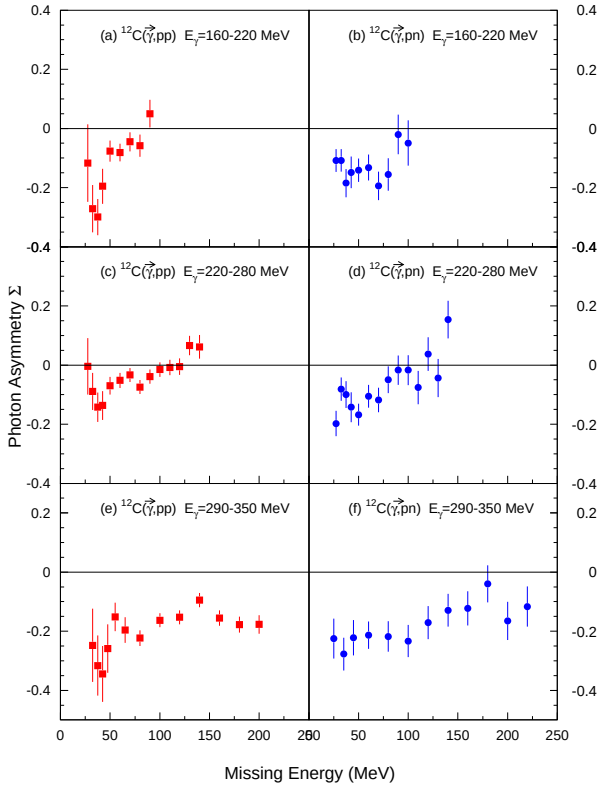

Fig. 3: Photon Asymmetry Σ plotted as a function of Missing Energy for the $^{12}C(\gamma,pp)$ (red squares) and $^{12}C(\gamma,pn)$ (blue circles) reactions, for three photon energy ranges.

Fig. 3 shows the photon asymmetry Σ as a function of E_m for both reaction channels, for the three E_γ ranges. The (γ,pp) data show a very strong negative peak for E_m <50 MeV. While this feature is attributable to the shoulder in the perpendicular yield, seen in Fig. 2, it is more clearly visible in the Σ spectrum. Indeed, for the highest E_γ range this structure is not at all obvious from the previous figure.

The strength of the observed (γ,pp) asymmetry at low E_m is greater than that of the (γ,pn) channel, in both the lowest and highest E_γ ranges. This discounts the possibility that the (γ,pp) reaction has a large contribution from initial (γ,pn) photon absorption followed by charge-exchange FSI in this E_m region, as FSI processes are not able to increase the magnitude of Σ. Together the observed structure and magnitude of Σ provide strong new evidence which implies that the (γ,pp) reaction proceeds through a direct process at low E_m.

At E_m >50 MeV the (γ,pp) asymmetry has a much smaller magnitude and for the two lowest E_γ ranges tends towards zero, or even slightly positive values, at high E_m.

The (γ,pn) asymmetry data are also negative but do not show the strong low E_m peak seen in (γ,pp) . Rather, they show a much more gradual E_m dependence, tending towards smaller magnitudes with increasing E_m. As in the (γ,pp) channel, the magnitude of the asymmetry at high E_m is largest in the highest E_γ range.

B Analysis of $(1p)^2$ and (1p)(1s) E_m Regions

As shown by previous work with unpolarised photons [14–18] the contributing reaction mechanisms change rapidly with E_m for both the (γ,pn) and (γ,pp) reactions. At E_m <40 MeV in ^{12}C the data for both reaction channels are well described by a direct two-nucleon emission process where the two nucleons are ejected from $(1p)^2$ orbitals. Between 40 and 70 MeV the data are predominantly due to direct two-nucleon emission from (1p)(1s) orbitals. Above 70 MeV more complex two-step processes become important.

For further analysis missing energy cuts of E_m <40 MeV and 40<E_m <70 MeV were applied to the data to emphasise direct two nucleon emission from $(1p)^2$ and (1p)(1s) orbits. In addition PiP and TOF angular bins were used to select events corresponding to quasideuteron kinematics. Four TOF solid angle bins were selected corresponding to both halves of the TOF stands EF and GH. Corresponding PiP solid angle bins were selected, using the method described by Yau *et al.* [19], accepting protons within $\pm 10^\circ$ of the mean proton polar angle $\overline{\theta_p}$ corresponding to the centre of each TOF solid angle bin and accepting the full azimuthal coverage of PiP. This process ensured that the analysed data sampled the peak of the (γ,NN) angular correlation and suppressed FSI events.

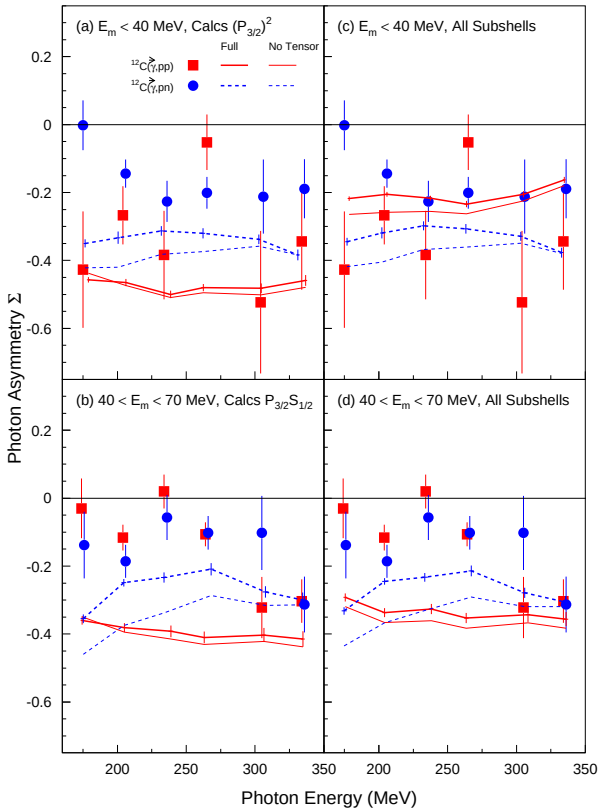

Fig. 4: Σ for E_m <40 MeV (a), (c) and for 40< E_m <70 MeV (b), (d) for ^{12}C(γ,pp) (red squares) and ^{12}C(γ,pn) (blue circles) as a function of E_γ , compared to Gent model calculations of $(1p)^2$ and (1p)(1s) two-nucleon emission. The calculations in (a) include only $(1p_{3/2})^2$ emission; (b) includes only $(1p_{3/2})(1s_{1/2})$ emission; (c) includes all $(1p)^2$ contributions; and (d) includes all (1p)(1s) contributions. The thick curves are the full calculations. The thin curves exclude tensor correlations. Error bars on the calculations indicate the statistical accuracy from sampling the experimental acceptances.

Fig. 4 shows Σ for(γ,pp) and (γ,pn) as a function of E_γ . The top two panels, (a) and (c), show data for E_m <40 MeV, whereas data for 40<E_m <70 MeV are shown in (b) and (d). The statistical accuracy of the low E_m (γ,pp) data is a factor of ∼2 worse than the (γ,pn) data. This is due to the lower cross sections for the (γ,pp) reaction.

In the low E_m region, the magnitude and shapes of Σ for the two reaction channels are quite different. As discussed in ref. [5], the shape of $\Sigma_{(\gamma,pn)}$ for ^{12}C in the Δ-resonance region is similar

to that for ^{2}H($\vec{\gamma}$,pn), although the ^{12}C magnitude is significantly smaller. In contrast $\Sigma_{(\gamma,pp)}$ generally has a flatter E_γ dependence and its magnitude generally exceeds that for $\Sigma_{(\gamma,pn)}$.

In the higher E_m region Σ has a smaller magnitude for both reaction channels than at lower missing energies and the differences between the two reaction channels are small.

Fig. 4 also shows the calculations obtained using the Gent model. The LH panels (a) and (b) show the predictions from the dominant $(1p_{3/2})^2$ and $(1p_{3/2})(1s_{1/2})$ contributions. These subshell contributions have by far the largest spectroscopic factors in each E_m region. Overall these calculations do not do very well at predicting the magnitude and energy dependence of Σ for either reaction channel.

In the low E_m region (a) the calculations predict that Σ for (γ,pp) is significantly larger than for (γ,pn) but the strength of the calculations is much larger than the experimental data in both channels. The calculations fail to show the drop in Σ at low E_γ in the (γ,pn) channel. There is a significant contribution from tensor correlations in the (γ,pn) channel whose inclusion brings the calculations closer to the experimental data. The effect of tensor correlations on the (γ,pp) asymmetry is negligible.

In the high E_m region (b) the calculations predict Σ values which greatly exceed the experimental data for both reaction channels. Σ for (γ,pp) is predicted to be larger than for (γ,pn) whereas the data show somewhat similar values for both reaction channels, with perhaps a slight indication that Σ for (γ,pn) exceeds (γ,pp) for E_γ<250 MeV.

The RH panels, (c) and (d), show the theoretical predictions when contributions from all nuclear subshells are taken into account. In both E_m regions there is little effect on the predictions for the (γ,pn) channel. However, large effects are seen in the (γ,pp) channel. The reason for this is the large predicted (γ,pp) cross sections for $(1p_{3/2})(1p_{1/2})$ and $(1p_{1/2})(1s_{1/2})$ emission. These subshell combinations are predicted to have very small asymmetries. Therefore, despite having small spectroscopic factors, the inclusion of these contributions significantly reduces the overall (γ,pp) asymmetry. In the low E_m region the effect is strong enough to make the predicted (γ,pp) asymmetry smaller than (γ,pn) .

Clearly the minor subshell contributions have an important role to play and their inclusion is necessary for complete calculations. However, at present their inclusion worsens the agreement with the experimental data. While there may be some uncertainty due to the choice of spectroscopic factors used, it is clear that considerable improvements in the theoretical models are necessary.

C Recoil Momentum Dependence

Previous work with unpolarised photons [14, 18] has examined the missing momentum dependence of the (γ,pp) and (γ,pn) reactions. In the absence of FSI the magnitude of the missing, or recoil, momentum is equal to that of the initial momentum P of the interacting pair, so that measurements of missing momenta allow access to the distribution of initial pair momenta. Plane wave models of direct two-nucleon emission predict a factorisation of the cross section into two parts: F(P) which can be obtained from the momentum wavefuctions of the two nucleons in a long-range mean field potential and S_{fi} which contains the effects of SRC. In distorted wave treatments this factorisation breaks down due to interference between contributing nuclear currents. Nevertheless calculations show that F(P) still dominates the kinematic dependence of the cross section [3]. Experimentally it is observed that the missing momentum distributions for both (γ,pn) and (γ,pp) reaction channels scale extremely well with calculated F(P) distributions [18]. Small residual differences at low momenta in the (γ,pp) channel are interpreted in terms of contributions from pairs in configurations other than the dominant $^1S_0$ and the relatively small amount of excess strength at high momentum justifies the assumption that FSI may be neglected.

In order to investigate whether the scaling with P applies to polarised cross sections the experimental Σ data were plotted as a function of missing momenta. If $\sigma_{||}$ and $\sigma_\perp$ have a similar missing momentum dependence then the asymmetry should not have a strong variation.

Fig. 5 shows the photon asymmetry for both the (γ,pp) and (γ,pn) reactions, averaged over E_γ=160–350 MeV, as a function of recoil momentum. In the low E_m region the dependence of Σ on recoil momentum for the ($\vec{\gamma}$,pn) reaction is not large. Note that there is very little strength at high recoil momentum and consequently the highest recoil momentum data point has poorer statistical accuracy. The error bars for the ($\vec{\gamma}$,pp) data are larger and more erratic so that no clear trend is apparent.

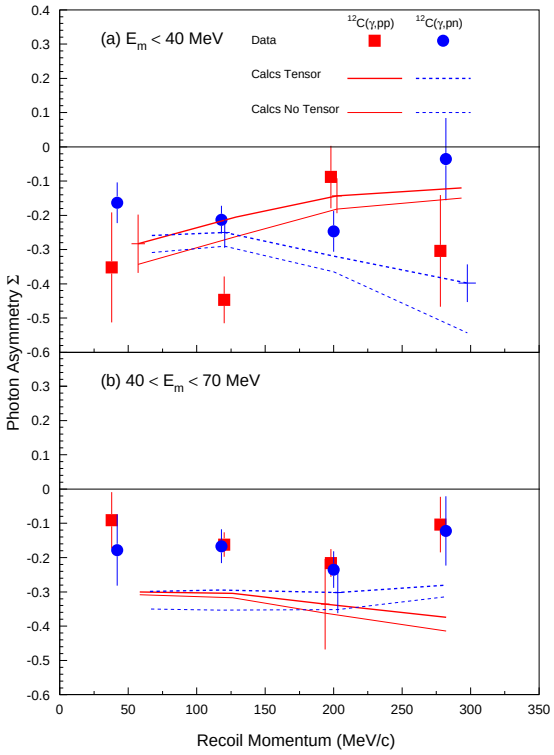

Fig. 5: Photon Asymmetry Σ plotted as a function of Recoil Momentum for the ^{12}C(γ,pp) (red squares) and ^{12}C(γ,pn) (blue circles) reactions, for two Missing Energy ranges. The curves are the results of calculations of (a) $(1p)^2$ and (b) (1p)(1s) two-nucleon emission obtained using the Gent unfactorised model, including contributions from all nuclear subshells. The thick curves are the full calculations. The thin curves exclude the contribution from tensor correlations. Sample error bars on the calculations indicate the statistical accuracy from sampling the experimental acceptances.

For the (γ,pn) reaction the Gent model predicts an asymmetry which increases slowly in magnitude with recoil momentum. This trend is in reasonable agreement with the first three data points, but is inconsistent with the highest recoil momentum data point. The effect of tensor correlations again brings the calculations closer to the experimental data.

For the (γ,pp) reaction the calculations predict a different behaviour in that the photon asymmetry falls in magnitude with increasing recoil momentum. Unfortunately the statistical accuracy of the (γ,pp) data is insufficient to allow more specific comment.

In the high E_m region $40<E_m<70$ MeV Σ shows very little recoil momentum dependence for either reaction channel. The theoretical predictions for both channels are rather flat, but as discussed previously are considerably larger than the experimental data.

The absence of any strong variation of Σ with recoil momentum, in the (γ,pn) channel and in the (γ,pp) channel in the high E_m region, indicates that both $\sigma_{||}$ and $\sigma_{\perp}$ have a similar dependence on F(P). This, in turn, gives confidence that integrating over recoil momentum, to investigate other observables, will not introduce any substantial bias into the spectra obtained. The statistical accuracy of the low E_m (γ,pp) data is too poor to allow such a conclusion to be drawn in that particular case.

D Angular distribution

Some limited information on the angular distribution of the ^{12}C($\vec{\gamma}$,pn) and ^{12}C($\vec{\gamma}$,pp) reactions has been obtained by plotting the differential cross sections for the four PiP/TOF solid angle bins, described previously, corresponding to quasideuteron kinematics.

Fig. 6 shows the dependence of $\frac{d\sigma_{||}}{d\Omega_{PiP}d\Omega_{TOF}}$ and $\frac{d\sigma_{\perp}}{d\Omega_{PiP}d\Omega_{TOF}}$ for the ^{12}C($\vec{\gamma}$,pp) and ^{12}C($\vec{\gamma}$,pn) reactions for E_m <40 MeV. As the experiment was designed principally to measure photon asymmetries the extracted cross sections have relatively large systematic uncertainties and have been multiplied by a common normalisation factor (1.5), as described by Powrie *et al.* [7], to facilitate comparison with the shapes of the theoretical predictions. The use of a common factor preserves the relative strengths of the parallel and perpendicular cross sections and the relative strengths of the ($\vec{\gamma}$,pp) and ($\vec{\gamma}$,pn) reaction channels.

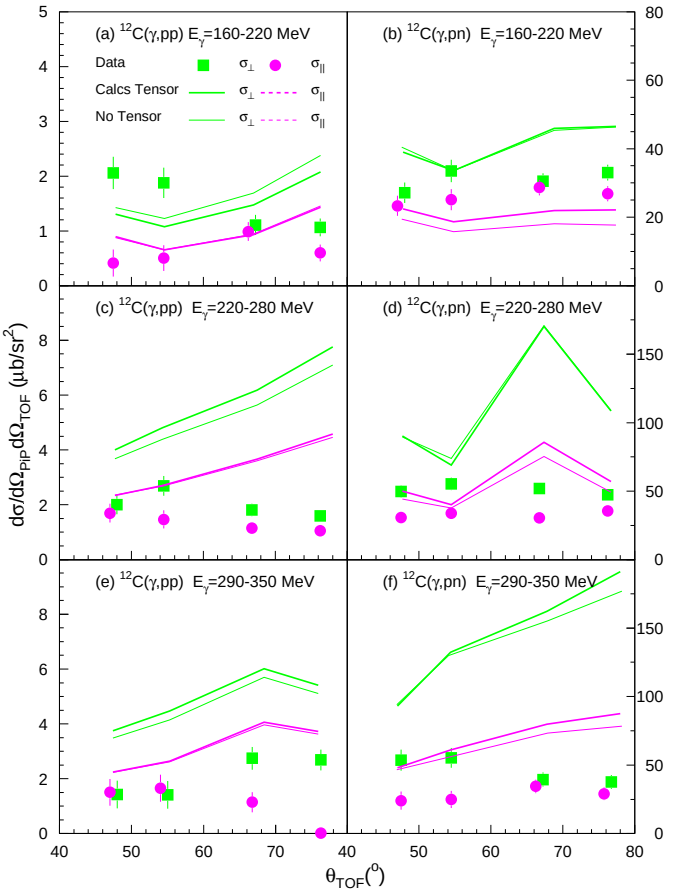

Fig. 6: Perpendicular (green) and parallel (purple) differential cross sections for the ^{12}C(γ,pp) and ^{12}C(γ,pn) reactions plotted as a function of the polar angle of the nucleon detected in TOF, for $E_m <$ 40 MeV. The curves are the results of calculations of $(1p)^2$ two-nucleon emission obtained using the Gent unfactorised model, including contributions from all nuclear subshells. The thick curves are the full calculations. The thin curves exclude the contribution from tensor correlations.

For the ($\vec{\gamma}$,pp) reaction there are significant differences in the shape of the angular distribution between $\sigma_{||}$ and $\sigma_\perp$. These differences are both energy and angle dependent. In general $\sigma_\perp$ is stronger than $\sigma_{||}$. As E_γ increases $\sigma_\perp$ peaks at more backward θ_{TOF} angles, whereas $\sigma_{||}$ peaks at more forward angles. Consequently the largest differences between $\sigma_\perp$ and $\sigma_{||}$ shift from θ_{TOF} ~50° for E_γ=160–220 MeV to ~70° for E_γ=290–350 MeV.

For the ($\vec{\gamma}$,pn) reaction $\sigma_\perp$ is stronger than $\sigma_{||}$ at all energies. The differences in shape between the angular distributions are much smaller in this channel, with $\sigma_{||}$ and $\sigma_\perp$ having rather similar distributions for the two lowest E_γ ranges. In the highest E_γ range $\sigma_\perp$ peaks at more forward θ_{TOF} angles than $\sigma_{||}$. This is the opposite behaviour to the (γ,pp) reaction.

The calculations presented are summed over all the contributing nuclear subshell combinations. They predict a strong dependence of both $\sigma_{||}$ and $\sigma_\perp$ on particle emission angle for both reactions. In general both $\sigma_{||}$ and $\sigma_\perp$ have similar trends for both reaction channels, increasing or decreasing together. However, in no case do the theoretical predictions give good agreement with the experimental data. The strong variation of the calculated cross sections with particle emission angles shows that this variable is a sensitive test for the calculations.

Fig. 7 shows the angular distribution of $\frac{d\sigma_{||}}{d\Omega_{PiP}d\Omega_{TOF}}$ and $\frac{d\sigma_\perp}{d\Omega_{PiP}d\Omega_{TOF}}$ for the ($\vec{\gamma}$,pp) and ($\vec{\gamma}$,pn) reactions for 40<E_m <70 MeV. The data have again been normalised by a factor of 1.5. For the ($\vec{\gamma}$,pp) reaction the differences between $\sigma_{||}$ and $\sigma_\perp$ are very small for the two lowest E_γ ranges. Both $\sigma_{||}$ and $\sigma_\perp$ have very similar shapes with $\sigma_\perp$ having the slightly larger magnitude. For E_γ=290–350 MeV $\sigma_\perp$ peaks at θ_{TOF} ~55°, whereas $\sigma_{||}$ is rather flat. $\sigma_\perp$ also has a significantly larger magnitude than $\sigma_{||}$ in this E_γ range.

For the ($\vec{\gamma}$,pn) reaction there is little difference between the angular distribution shapes of $\sigma_{||}$ and $\sigma_\perp$ in the lowest E_γ range. $\sigma_\perp$ is stronger than $\sigma_{||}$ at all measured angles. However for both the higher E_γ ranges $\sigma_\perp$ is peaked at central angles, whereas $\sigma_{||}$ is rather flat.

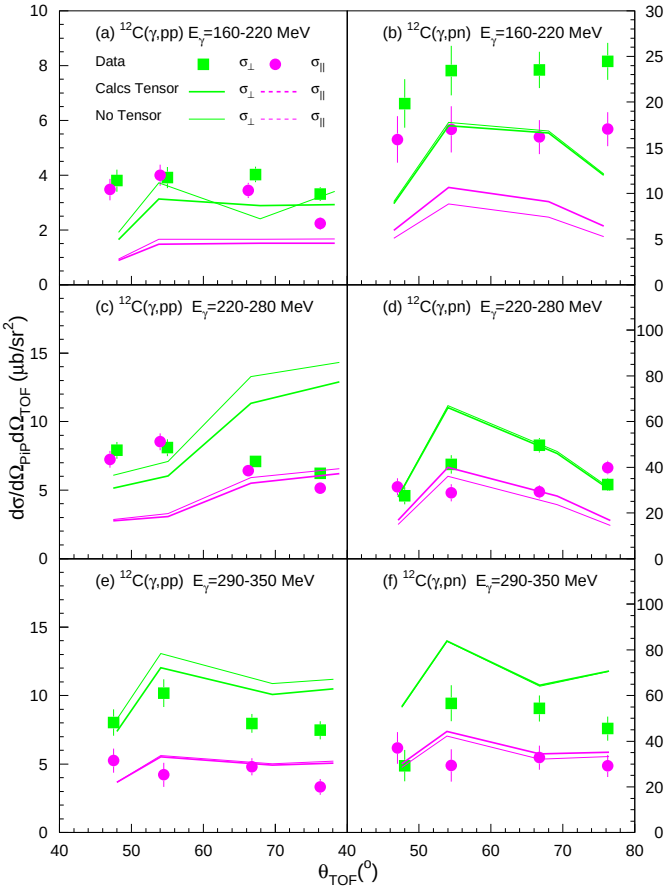

Fig. 7: Perpendicular (green) and parallel (purple) differential cross sections for the ^{12}C(γ,pp) and ^{12}C(γ,pn) reactions plotted as a function of the polar angle of the nucleon detected in TOF, for 40<E_m <70 MeV. The curves are the results of calculations of (1p)(1s) two-nucleon emission obtained using the Gent unfactorised model, including contributions from all nuclear subshells. The thick curves are the full calculations. The thin curves exclude the contribution from tensor correlations.

Theoretical predictions of the Gent model, again including all subshell contributions, are also shown in Fig. 7. The shapes of the theoretical distributions give a somewhat better agreement with the trends of the experimental data than in the lower E_m region, but still could not be described as giving a good account of the data.

E Two-Step Processes

In the E_m range above 70 MeV two-step processes are expected to dominate the cross section [16, 17]. A comparison of measured E_m spectra with calculations carried out using the Valencia model [16] indicated that above ~250 MeV two-step processes dominate both reaction channels, with the most important process being initial pion production on a nucleon followed by pion reabsorption on a pair of nucleons. A separate study by Harty *et al.* [17], which examined the recoil momentum distributions for (γ,pp) and (γ,pn) reactions for E_m=100–200 MeV, provided additional evidence to suggest that this E_m region is populated by two-step processes.

Fig. 8 shows the E_γ dependence of Σ for data with E_m >70 MeV, averaged over the whole angular acceptance of PiP and TOF. There is little difference in the results for both reaction channels as might be expected if both reactions are dominated by similar two-step processes. Σ is small for both channels for E_γ<270 MeV. Above this energy the magnitude increases rapidly for both reaction channels, reflecting the change in the dominant reaction mechanism, as suggested in ref. [16], from two-nucleon absorption followed by FSI to pion photoproduction followed by pion reabsorption.

As FSI processes cannot increase the photon asymmetry, the large asymmetry values observed must result from the initial pion production process. It is known that pion production on the proton has large asymmetry values: $\Sigma \sim -0.35$ for p($\vec{\gamma}$,π^+)n and $\Sigma \sim -0.45$ for p($\vec{\gamma}$,π°)p at $E_\gamma \sim 300$ MeV [20]. Negative pion production has been measured in the ^{16}O($\vec{\gamma}$,π^-p) reaction at $E_\gamma = 293 \pm 20$ MeV, over a range of proton angles 28–140° and pion angles 35–115° [21]. This

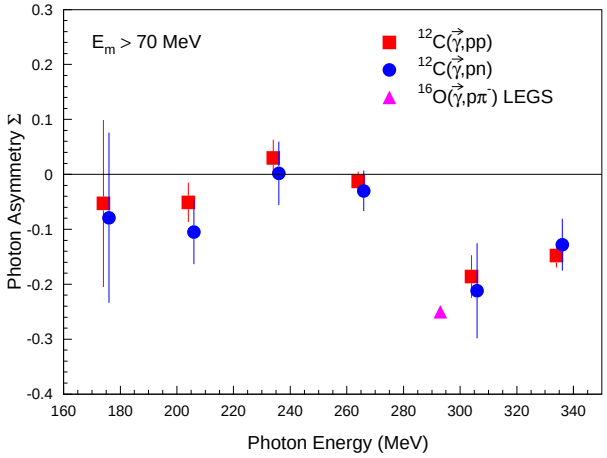

Fig. 8: Photon Asymmetry Σ, for events with E_m >70 MeV, plotted as a function of E_γ for $^{12}C(\gamma,pp)$ (red squares) and $^{12}C(\gamma,pn)$ (blue circles). Also shown for comparison is Σ for the $^{16}O(\gamma,\pi^-p)$ reaction (purple triangle) measured at LEGS [21].

reaction also has a reasonably strong photon asymmetry $\Sigma \sim -0.25$ which is likely to stem from initial quasifree π^- production on bound neutrons, although the asymmetry of the initial process is likely to be reduced somewhat by Fermi smearing in ^{16}O.

In photo-induced two-nucleon emission a similar transfer of photon asymmetry from an initial quasifree pion to the final nucleon pair is possible since the π^+ absorption cross section on the deuteron is largest at forward-backward angles [22].

5. CONCLUSIONS

Linearly polarised photons provide a unique and relatively new tool to explore two-nucleon emission reactions. While polarised photon sources have been available for over 30 years and some pioneering work has examined the E_γ dependence of Σ for ($\vec{\gamma}$,NN) reactions in a range of light nuclei, the present work is the most detailed study of this process so far.

An important finding is the discovery of a strong peak in the magnitude of Σ in the ($\vec{\gamma}$,pp) channel at low E_m, where contributions from direct two-proton knockout are expected. This observation indicates that this channel is dominated by a strong direct knockout mechanism at low E_m.

The data were compared with state-of-the-art theoretical calculations of two-nucleon knockout using a model developed by the Gent group. These calculations were carried out using an unfactorised distorted wave formalism which included the effects of central and tensor SRC. The calculations included contributions from all possible nucleon orbits and were averaged over the acceptance of the experiment. Nevertheless the calculations do not adequately describe the photon energy or angular dependence of either the direct ($\vec{\gamma}$,pp) or ($\vec{\gamma}$,pn) processes.

Measurements of Σ for E_γ >250 MeV, and E_m >70 MeV, where two-step processes are known to dominate the (γ,NN) reactions, are seen to reflect the asymmetry of the initial photoabsorption process. It is suggested that the initial asymmetry is preserved to a large degree in the final state processes which are important at these energies.

Overall this work has illustrated the importance of accessing polarisation observables in the study of photonuclear reactions. The present data are already providing new constraints for theoretical models of direct two-nucleon emission and have also indicated interesting physics at high E_m. However the present measurements are restricted by poor statistical accuracy and improved experiments are required for a detailed exploration of the dependence of the nuclear response to photon polarisation. Better statistical accuracy and higher resolution are needed to study the properties of individual states in the residual nucleus. This is a necessary step to unravelling the strong angular momentum dependence of the polarisation observables, glimpsed in the present limited angular distributions. There is also a need for measurements over a wider range of photon energies to investigate the strong photon energy dependence of the photon asymmetry which may provide information on how the basic contributing mechanisms depend on the incident photon energy. Finally there is scope to extend the present work to a range of light nuclei to explore the dependence of polarisation observables on nuclear density.

ACKNOWLEDGMENTS

This work has been supported by grants from the UK EPSRC, the British Council, the DFG (Mu 705/3, SSP 1043), BMFT (06 Tü 656), DAAD (313-ARC-IX-95/41), the EC (SCI.0910.C(JR)) and NATO (CRG 970268).

REFERENCES

[1] S.J. Hall *et al.*, Nucl. Inst. Meth. A **368** (1996) 698;
I. Anthony *et al.*, Nucl. Inst. Meth. A **301** (1991) 230
[2] H. Herminghaus, Proc. of the Linear Accelerator Conference, Albuquerque, USA, 1990;
T. Walcher, Prog. Part. Nucl. Phys. **24** (1990) 189
[3] J. Ryckebusch *et al.*, Phys. Rev. **C57** (1998) 1319;
J. Ryckebusch *et al.*, Phys. Lett. B **291** (1992) 213;
L. Machenil *et al.*, Phys. Lett. B **316** (1993) 17;
J. Ryckebusch *et al.*, Nucl. Phys. A **568** (1994) 828;
M. Vanderhaegen *et al.*, Nucl. Phys. A **580** (1994) 551
[4] S. Boffi, C. Giusti, F. D. Pacati and M. Radici, Electromagnetic Response of Atomic Nuclei, Oxford University Press (1996); C. Giusti and F. D. Pacati, Nucl. Phys. A **641** (1998) 297;
S. Boffi *et al.*, Nucl. Phys. A **564** (1993) 473;
C. Giusti *et al.*, Nucl. Phys. A **546** (1992) 607
[5] S. Franczuk *et al.*, Phys. Lett. B **450** (1999) 332
[6] I.J.D. MacGregor, Proc. 4th Workshop on Electromagnetically Induced Two-Hadron Emission, Granada 1999, Ed. C. Garcia-Recio, P. Grabmayr, A. M. Lallena and R. O. Owens, pp. 339–352
[7] C.J.Y. Powrie *et al.*, Phys. Rev. C, in press
[8] I.J.D. MacGregor *et al.*, Nucl. Inst. Meth. A **382** (1996) 479
[9] P. Grabmayr *et al.*, Nucl. Inst. Meth. A **402** (1998) 85;
T. Hehl *et al.*, Nucl. Inst. Meth. A **354** (1995) 505
[10] S. Wunderlich and F. A. Natter, internal report (1998), University of Tübingen;
F. A. Natter, Proc. 4th Workshop on Electromagnetically Induced Two-Hadron Emission, Granada 1999, Ed. C. Garcia-Recio, P. Grabmayr, A. M. Lallena and R. O. Owens, pp. 59–69;
F. A. Natter *et al.*, to be published.
[11] C.C. Gearhart, Ph.D. Thesis, University of Washington (1994);
W. Dickhoff, private communication
[12] D.G. Ireland, I.J.D. MacGregor and J. Ryckebusch, Phys. Rev. C. **59** (1999) 3297
[13] D.G. Ireland and G. van der Steenhoven, Phys. Rev. C. **49** (1994) 2182
[14] J.C. McGeorge *et al.*, Phys. Rev. C **51** (1995) 1967
[15] S.N. Dancer *et al.*, Phys. Rev. Lett. **61** (1988) 1170
[16] T. Lamparter *et al.*, Z. Phys. A **355** (1996) 1
[17] P.D. Harty *et al.*, Phys. Lett. B **380** (1996) 247
[18] D.P. Watts *et al.*, Phys. Rev. C **62** (2000) 014616
[19] T.T.-H. Yau *et al.*, Eur. Phys. Jour. A **1** (1998) 241
[20] F.A. Berends *et al.*, Nucl. Phys. B **4** (1967) 54
[21] K. Hicks *et al.*, Phys. Rev. **C55** (1997) R12;
ibid **C61** (2000) 054609
[22] H.J. Weyer, Phys. Rep. **195** (1990) 295